J Mater Sci (2006) 41:5194–5199
DOI 10.1007/s10853-006-0441-9

Mechanical properties and interfaces of zirconia/nickel in micro - and nanocomposites

S. Lopez-Esteban · T. Rodriguez-Suarez · F. Esteban-Betegón · C. Pecharromán · J. S. Moya

Received: 30 September 2005 / Accepted: 1 February 2006 / Published online: 29 July 2006

Abstract The effect of processing parameters on the hardness and toughness of yttria-doped zirconia/nickel nanocomposites is reported. The experimental procedure consists in the deposition of nickel nanoparticles—previously obtained from nickel nitrate salts—on the surface of the zirconia powders. Slight changes in the proposed processing route (i.e. drying temperature of powders) gave rise to a noticeable decrease in the hardness (15–20%). However, no effect was observed on the toughness values in the studied composition range (0–30 vol% Ni). These results have been explained in terms of the nickel particle size distribution and agglomeration due to differences in the melting temperature of nickel nanoparticles, and because of epitaxial growth of nickel on the zirconia surface. For comparison purposes, samples obtained following a conventional wet-processing route starting from micrometric nickel and yttria-doped zirconia powders were prepared. In this case, the toughness is strongly dependent on the nickel fraction. This fact has been related to the weak bonding between metal and ceramic particles.

Introduction

Because the properties of nanoparticles depend so closely on their size, as well as size distribution and morphology, techniques for controlling the growth of these tiny structures is today of great interest to materials researchers [1]. The yttria-doped zirconia/nickel system could be the perfect candidate to model the mechanical properties of ceramic/metal micro- and nanocomposites. First of all, the mismatch in the thermal expansion coefficients between nickel and zirconia is very small (less than 5%) [2] and therefore residual thermal stresses are minimal. Also the grain growth of zirconia during sintering is almost negligible [3]. This fact minimizes the metal coarsening in the final compact. Secondly, the elastic moduli are nearly identical (200 GPa). Finally, the lattice parameter of zirconia is $\sqrt{2}$ times that of nickel, with a difference of 2%. This small misfit allows a satisfactory epitaxial growth of nickel on zirconia. Besides, among its possible applications as structural material [4], nowadays zirconia/nickel composites attract much attention because of its application in the fabrication of solid oxide fuel cells with a required lifetime longer than 40,000 h [5].

The aim of this work was to compare zirconia/nickel composites obtained by different methods using the same zirconia powders as matrix. Composites formed by zirconia and nickel inclusions with average particle size in the range of nanometers (10–100 nm) and micrometers (1–2 μm) have been studied.

Experimental

Materials

The following commercially available powders have been used as raw materials: (1) Tetragonal zirconia polycrystals (3Y-TZP, 3 mol% Y_2O_3; TZ-3YS, Tosoh Corp.), with an average particle size of $d_{50} = 0.26 \pm 0.05$ μm and a BET specific surface area of 6.7 m^2/g;

S. Lopez-Esteban (✉) · T. Rodriguez-Suarez · F. Esteban-Betegón · C. Pecharromán · J. S. Moya
Instituto de Ciencia de Materiales de Madrid (ICMM), Consejo Superior de Investigaciones Científicas (CSIC), Cantoblanco, Madrid 28049, Spain
e-mail: slopez@icmm.csic.es

(2) nickel(II) nitrate hexahydrate (Merck, Germany, 99.0% purity, $Ni(NO_3)_2{\cdot}6H_2O$); (3) nickel ultrafine powders (NFP-201; Kawatetsu Mining Co., Ltd), 99.9 wt% purity, oxygen content 0.5 wt%, average particle size $d_{50} = 1.70 \pm 0.05$ μm and a BET specific surface area of 3.02 m^2/g.

Processing

Nanocomposites

Zirconia/nickel nanocomposites have been prepared by deposition of nickel nanoparticles on the surface of the ceramic powders [6]. Nickel nitrate salt powders were dispersed in absolute alcohol by ultrasonic agitation in a suitable volume of alcohol to achieve total dilution. Zirconia powder was then added and the suspension was milled for 24 h with zirconia balls. The mixture was dried under vacuum at either 100 °C or 300 °C and then calcined at 600 °C for 2 h in air to obtain ZrO_2/NiO powders. The resulting powder was sieved down to 100 μm. Finally, the NiO was reduced to metallic nickel in a 90% Ar/10% H_2 atmosphere at 500 °C for 2 h Subsequently, the powders were isostatically pressed at 200 MPa. The resulting bars (5 mm diameter and 50 mm long, aprox.) were fired in a 90% Ar/10% H_2 atmosphere in two steps: (1) 500 °C for 2 h in order to reduce the NiO present in the surface of the starting Ni particles, and (2) at 1415 °C for 2 h for final sintering. The heating and cooling rate was kept at 600 °C/h.

Microcomposites

Zirconia/nickel microcomposites were obtained following a conventional wet processing route [3]. The average Ni particle size was 1.5 μ. 3Y-TZP/Ni suspensions with 70 wt% solid content were prepared using distilled water as liquid media and a 3 wt% addition of an alkali-free organic polyelectrolyte as surfactant. Relative proportion of Ni ranges between 2.5 vol% and 40 vol%. The mixtures were homogenized by milling with zirconia balls for 24 h. and then dried at 90 °C for 24 h. The resulting powders were ground in an agate mortar and subsequently passed through a 100 μm sieve. Powders were isostatically pressed and sintered following the same procedure as described for nanocomposites.

Characterization

X-ray diffraction analysis (XRD) of the powders was performed for phase identification (Philips PW 1710) and for Ni crystallite size determination (Philips ŕXPert) based on the (111) peak (28.223°) line width. The average grain size of Ni was roughly estimated from X-ray line broadening according to the Scherreŕs equation, $d = 0.9\lambda/\beta\cos\theta$, where λ is the wavelength of the incident X-ray radiation ($CuK\alpha_1$, $\lambda = 1.5405981$ Å) and θ is the scattering angle. The corrected peak half width, β, was obtained according to the Warren formula ($\beta^2 = B_m^2 - B_s^2$) being B_m the measured peak width and B_s the instrumental peak width [7, 8].

The microstructure of fired specimens was studied on surfaces polished down to 1 μm by optical microscopy and scanning electron microscopy (SEM, model DSM 960, Zeiss Thornwood, NY). The Ni particle size distribution in the specimens was measured from transmission electron microscopy (TEM) images (JEOL microscope, model FXII, JEM 2000, operating at 200 kV) for powdered samples. For high resolution transmission electron microscopy (HRTEM), a JEOL ARM microscope operating at 1250 keV was used for sintered samples.

The Vickers hardness, H_V, and fracture toughness, K_{IC}, were measured using a Vickers diamond indenter (Leco 100-A, St. Joseph, MI) on polished surfaces, with applied loads of 9.8 N and 490 N, respectively. The latter was chosen in order to obtain well-developed cracks (without chipping) starting at the four corners of the indentation impression. The corresponding crack sizes were determined using an optical microscope (Leica DMRM, Cambridge, UK). The fracture toughness was calculated using the formula given by Miranzo and Moya [9].

Results and discussion

Well dispersed zirconia–nickel nano- and microcomposites have been prepared. Toughness decreases significantly (up to 20%) in microcomposites with high Ni contents. However, in the case of nanocomposites toughness presents values nearly constant (~5.0 MPa $m^{1/2}$) as observed in Fig. 1a.

The behavior of hardness as a function of Ni content also presents large differences between micro- and nanocomposites (Fig. 1b). In microcomposites, a linear softening with increasing nickel contents was observed, as it corresponds to the rule of mixtures. However, nanocomposites present a notable hardness increase (30%) for low nickel content (2.5–7.5 vol%) to progressively reduce their hardness. For concentrations higher than 15 vol% Ni, hardness follows the rule of mixtures both for micro- and nanocomposites. The nanocomposites hardness versus nickel content

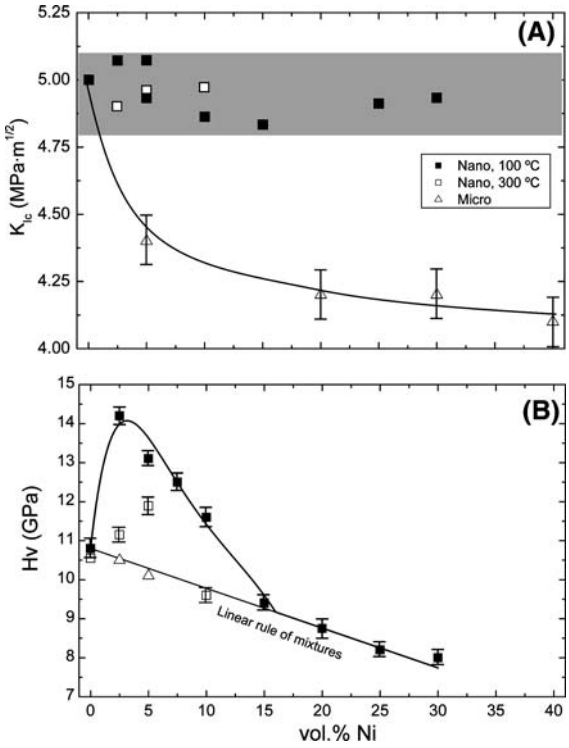

Fig. 1 Toughness (**a**) and Vickers hardness (**b**) of ZrO_2/Ni composites for increasing volume contents of Ni nano - and microparticles

(Fig. 1b) is in good agreement with the theoretical model proposed by Pecharroman et al. [10].

It has been found that small changes in the experimental procedure of obtaining zirconia–nickel nanocomposites have a great influence on the resultant microstructure and mechanical properties. Fig. 2 shows the XRD patterns obtained from powders dried at 100 °C and 300 °C. The average grain size of nickel was roughly estimated from X-ray line broadening according to the Scherrer's equation. The results obtained are 30 ± 3 nm and 17 ± 3 nm for powder dried at 100 °C and 300 °C, respectively. Thus, a significant decrease in the average nickel grain size (around 50%) has occurred as the drying temperature of the powder increased.

This result was confirmed by TEM as observed in the details shown in Fig. 3a and Fig. 3b. Remarkable differences in microstructure were found. Samples obtained from powder dried at 100 °C present a homogenous and narrow grain size distribution of metal particles (Fig. 3c). However, samples dried at 300 °C display nickel aggregates heterogeneously distributed (Fig. 3d).

From a close observation of these agglomerates, we can infer that melting processes have taken place on metal nanoparticles. It is well established experimentally that the particle melting point, T_m, of nanoparticles (< 100 nm) decreases linearly with a decreasing radius compared to that of the bulk (1455 °C, in the case of nickel) [11, 12]. Considering the results reported by Nanda [13], the expected melting point depression for the nickel nanoparticles corresponding to the samples dried at 100 °C is about 25 °C, that is, $T_{m,100\,^\circ C} \approx$ 1430 °C. In the case of samples dried at 300 °C, the corresponding melting point depression is about 65 °C, that is, $T_{m,300\,^\circ C} \approx 1390$ °C. Since all the samples were sintered at 1415 °C, the ones dried at 100 °C have clearly stayed below their melting temperature, while the ones dried at 300 °C have reached their corresponding melting point, forming larger particles. This fact is consistent with the lower hardness values of composites obtained from powders dried at 300 °C, as predicted by the theoretical model proposed by Pecharroman et al. [10].

Additionally, noticeable differences in microstructure were found between 3Y-TZP/Ni micro- and nanocomposites in samples with high Ni content. Nanocomposites reach high densities (>98% th.) in the whole range of the compositions studied (Fig. 4a). However, microcomposites present a significant fraction of porosity (5–15%) mainly associated to the nickel microparticles (Fig. 4b). This microstructural feature can be successfully explained from the information extracted from the HRTEM studies of the interface. Nickel nanoparticles present a faceted aspect, with curved lines flanking sharp interfaces, and a good epitaxy between Ni and ZrO_2, as it can be observed in Fig. 4c, in contrast with the porous structures found in microcomposites (Fig. 4d). This behavior was observed in all the nanocomposite samples in the range studied (up to 30 vol% Ni) even in samples with high metal content (>10 vol% Ni) where nickel

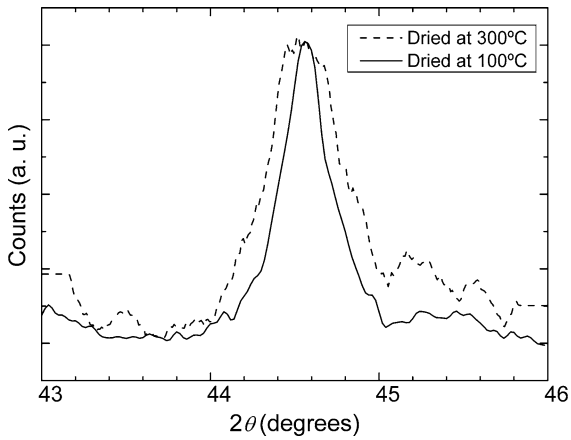

Fig. 2 X-ray diffractograms of zirconia/nickel powders (5 vol% Ni) after drying at (**a**) 100 °C (continuous line), and (**b**) at 300 °C, (dashed line). A significant increase in Ni grain size (about 50%) has occurred along with the drying temperature

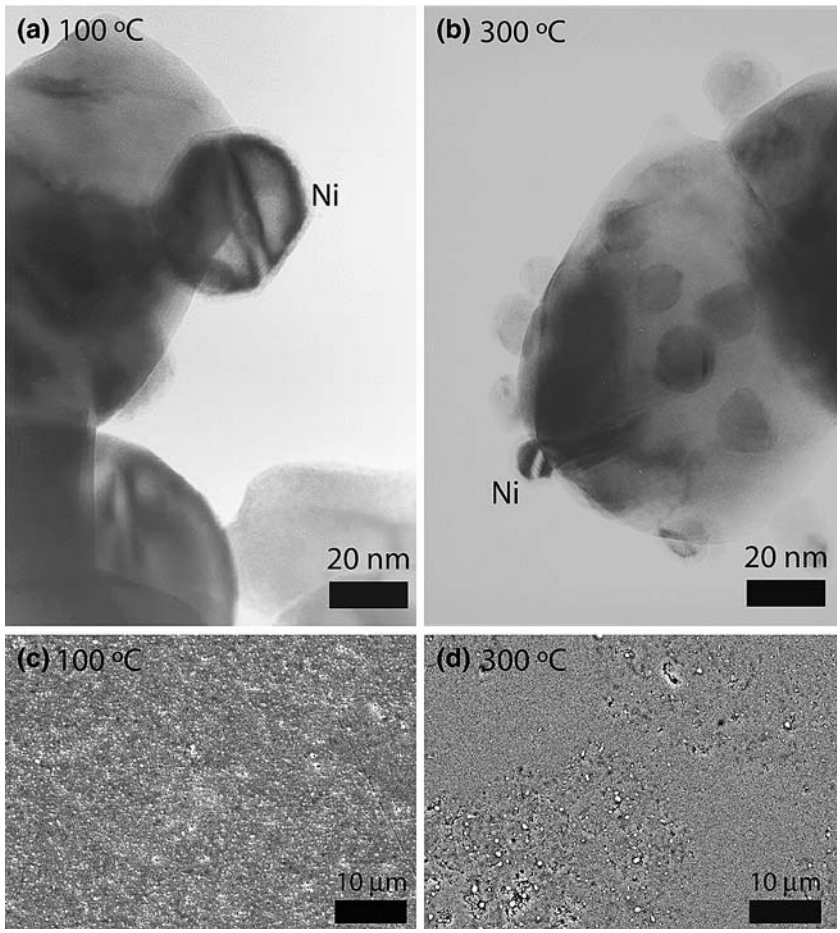

Fig. 3 TEM images corresponding to 5 vol% Ni sample powder dried at (**a**) 100 °C and (**b**)300 °C. Figs. (**c**) and (**d**) show SEM micrographs corresponding to sintered samples (10 vol% Ni nano) after dried at 100 °C and 300 °C, respectively

nanoparticles coalesce and form larger particles (>100 nm). In Fig. 4c and Fig. 4e, excellent ceramic/metal bonding and lattice matching in $ZrO_2(110)$/Ni(100) interfaces is observed. According to the HRTEM observations, microcomposites never displayed lattice matching in ZrO_2/Ni interfaces (Fig. 4f). The large amount of porosity associated to nickel particles and practically no matching between Ni and zirconia lattices in microcomposites justify the mechanical properties found (K_{IC}).

Most of the grain growth models proposed for spherical particles [14] can be expressed as follows:

$$x/R = (k \cdot t)^{(1/n)} \cdot R^{-(m/n)}$$

where R stands for particle radius, x for the neck size, t for the time, k is a constant and m and n are integers which depend on the kind of grain growth mechanism. In the case of evaporation-condensation, $m = 2$, $n = 3$; for volume diffusion $m = 3$, $n = 5$; for surface diffusion $m = 4$, $n = 7$; and for plastic flow $m = 1$, $n = 2$. Generally speaking, for an arbitrary case, the grain growth will depend on both the k value and the exponents m and n. However, because the evaporation–condensation has the most negative m/n exponent, there must be a critical R value below which the dominant grain growth mechanism must be evaporation–condensation. Observations by high resolution electron microscopy have shown the existence of nanoparticles arrays [11], formed because nanoparticles become elongated in the direction towards each other before they create an actual contact. Therefore, in order to explain this evidence, the critical R value must lay in the range of nanometers.

We consider that the origin of the good degree of epitaxy in 3Y-TZP/Ni nanocomposites can be due to two reasons: (1) a very good lattice matching between ZrO_2 and nickel (taking into account a 45° rotation in one of the crystals) and (2) the evaporation-condensation grain growth mechanism operating in metallic nanoparticles during sintering [11]. It should be noted that the temperature range to verify this process is very close, but under the melting point of nanoparticles. Therefore, the optimal conditions to obtain the best epitaxy requires a carefully temperature sintering control. The combined effect of these factors produces

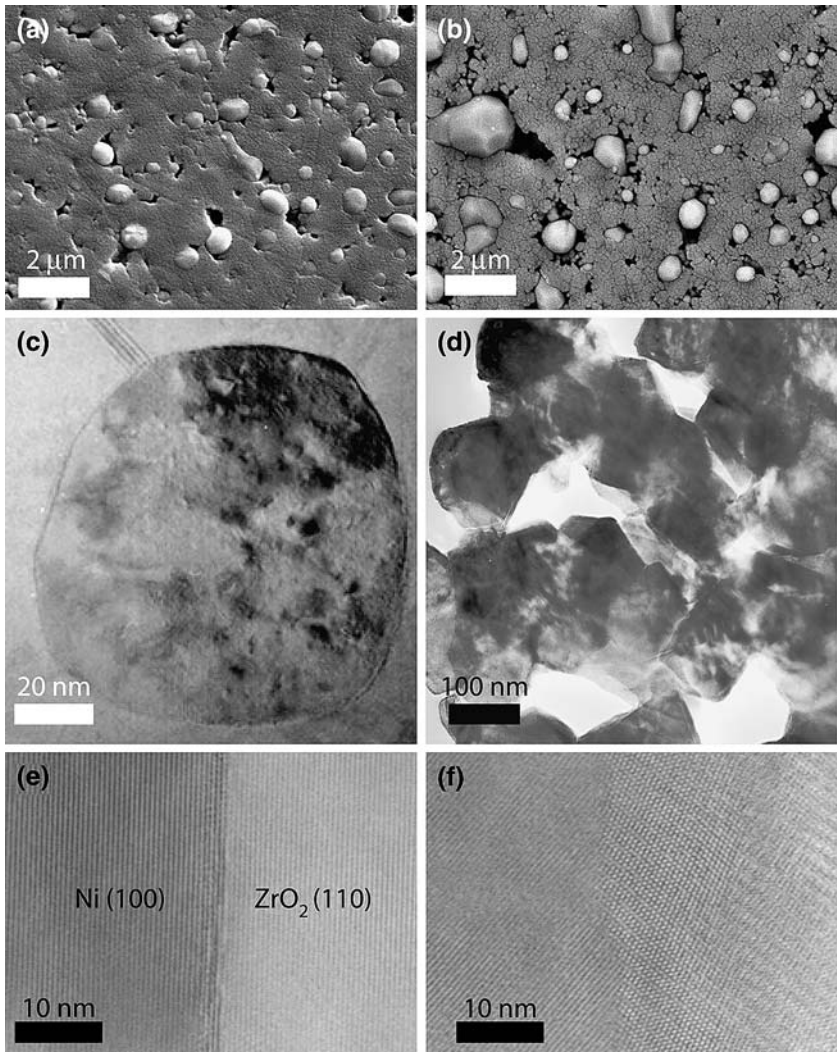

Fig. 4 SEM micrographs corresponding to 25 vol% Ni samples thermally etched in H_2/Ar at 1240 °C for 0.5 h, in a nano- and a microcomposite (**a** and **b**, respectively). TEM images of nickel embebbed in zirconia matrix in a nano- and a microcomposite (**c** and **d**, respectively). TEM images of zirconia/Ni interfaces in a nano- and a microcomposite (**e** and **f**, respectively.)

a real epitaxial growth of Ni crystals on ZrO_2 submicron grains. In fact, such kind of epitaxial interfaces can be successfully simulated by *ab initio* calculations so that the obtained numerical results are reliable in such particular systems.

According to Beltran et al. [15, 16], the results of the calculation indicate that in the ZrO_2(001)/Ni(001) interface, a separation work of approximately 5000–5700 mJ m^{-2} was determined. These values are similar to the separation work of bulk Ni and much smaller than that of pure zirconia. Conversely, the ZrO_2(011)/Ni(001) interface presents a separation work of only 900 mJ m^{-2}. This low value can be related to the poor atomic match that this interface presents. These low separation works can explain the decrease of the K_{IC} values found mainly in microcomposites. It can be stated that the work of separation of a strong interface as Al_2O_3/Nb (E_{sep} = 9800 mJ·m^{-2}) [17] indicates that it is about twice as strong as the ZrO_2/Ni interface studied. Therefore, it seems clear that nickel cannot substantially reinforce—by a bridging mechanism, for instance—and it decreases the toughness of zirconia in microcomposites instead.

Conclusions

It has been found that small changes in the processing of 3Y-TZP/nNi powder significantly affect the nickel nanoparticles grain size leading to lower hardness values in the sintered composites. However, due to the good interfacial bonding and low porosity in 3Y-TZP/nNi nanocomposites, the value of toughness is not sensitive to processing parameters or nickel fraction.

Acknowledgements This research has been supported by the European Union under project IP NANOKER (NMP3-CT-2005-515784), by the Spanish Ministry of Education and

Science under the project MAT2003-04199-C02-01 and by the autonomous region of Madrid under project GR/MAT/0432/2004. S. Lopez-Esteban has been supported by the Spanish Ministry of Education and Science under Ramón y Cajal Program.

References

1. Dowling A (2004) Nanoscience and nanotechnologies: opportunities and uncertainties, The Royal Society & The Royal Academy of Engineering
2. Tien JK and Howson TE (1981) Kirk-Othmer encyclopedia of chemical technology, vol. 15, 3rd edn. John Wiley & Sons, Inc., USA, p 788
3. Lopez-Esteban S, Bartolome JF, Moya JS, Tanimoto T (2002) J Mater Res. 17:1592
4. Shiota I and Miyamoto Y (eds.), (1997) in Proc. 4th Int Symposium Funct Grad Mater., Tsukuba, Japan, 1996, Elsevier Science
5. Lashway RW (2005) MRS Bulletin 30:581
6. Esteban-Betegon F, Lopez-Esteban S, Requena J, Pecharroman C, Moya JS, Conesa JC (2006) J Am Ceram Soc 89:144
7. Srdic V, Winterer M, Möller A, Miehe G, Hahn H (2001) J Am Ceram Soc 84:2771
8. West AR (1987) Solid state chemistry and its applications. John Wiley and Sons, Norwich, p 173
9. Miranzo P, Moya JS (1984) Ceram Int 10:147
10. Pecharroman C, Esteban-Betegon F, Bartolome JF, Richter G, Moya JS (2004) Nanoletters 4:747
11. Gryaznov VG, Trusov LI (1993) Prog Mater Sci 37:289
12. Vallée R, Wautelet M, Dauchot JP, Hecq M (2001) Nanotechnology 12:68
13. Nanda KK (2005) Appl Phys Lett 87:021909
14. Kingery WD, Bowen HK, Ulhmann DR (1976) Introduction to ceramics. John Wiley & Sons, New York, p 472
15. Beltran JI, Gallego S, Cerda J, Moya JS, Muñoz MC (2003) Phys Rev B 68:075401
16. Pecharroman C, Beltran JI, Esteban-Betegon F, Lopez-Esteban S, Bartolome JF, Muñoz MC, Moya JS (2005) Z Metallkd 96:507
17. Batirev IG, Alavi A, Finnis MW, Deutsch T (1999) Phys Rev Lett 82:1510